# Metal-to-semiconductor conductivity transition in indium tin oxide thin films via thermally induced structural rearrangement

© N.S. Parashchuk[1], Yu.E. Bonyushkin[1,2], A.D. Kurilov[1], A.A. Morozov[1], A.V. Nuriev[1], S.A. Stakharniy[1], D.N. Chausov[1]

[1] Prokhorov Institute of General Physics, Russian Academy of Sciences, 119991 Moscow, Russia
[2] State university of education, 105005 Moscow, Russia

E-mail: parashchuk.ns@mail.u

*Received June 1, 2026*
*Revised July 6, 2026*
*Accepted July 15, 2026*

This study investigates the effect of static and dynamic annealing on the electrical and microstructural properties of indium tin oxide films deposited in inert and oxygen-containing atmospheres. The presence of oxygen during deposition is found to induce an insoluble SnO phase, which gives rise to metallic conductivity at low temperatures and a sharp transition to semiconducting behavior upon annealing. Furthermore, oxygen present during deposition is shown to form stable tin oxide clusters that remain undissolved at 300 °C and determine the non-monotonic temperature dependence of electrical conductivity.

**Keywords:** thin films, structural-phase transition, surfaces, thermal annealing.

DOI: 10.61011/SC.2026.04.64076.9976

## 1. Introduction

Indium oxide $In_2O_3$, doped with tin Sn (hereinafter referred to as — ITO), is a reference material for the development of transparent electrodes due to the ability to achieve high conductivity with transparency preservation [1–3]. Physical properties of ITO films depend on the interaction of multiple factors, among which one can distinguish the lattice defects, the condition of the doping impurity and structure stoichiometry [4–6]. The initial $In_2O_3$ is a degenerate semiconductor of *n*-type, and at the expense of a relatively weak bond of In−O it is possible that defects arise in the form of oxygen vacancies. In this case the composition may be presented as $In_2O_{3-x}(V)_x$, where $V$ — double-charged vacancy. Concentration of $V$ depends on the conditions of deposition, and each $V$ yields two conduction electrons, providing in the undoped $In_2O_3$ for the concentration of free carriers $\sim 10^{19}\,cm^{-3}$. Doping with tin makes it possible to introduce additional donors up to $\sim 10^{21}\,cm^{-3}$ at the expense of substitution of indium ion $In^{3+}$ with tin ion $Sn^{4+}$, which causes conductivity $\sim 10^4\,S\cdot cm^{-1}$, and then the ITO composition may be presented as $In_{2-y}Sn_yO_{3-2y-x}(V)_x$ [7,8].

Deposition of ITO films in the inert atmosphere of Ar makes it possible to form the films with excessive oxygen vacancies and high concentration of free carriers, however, due to low mobility of carriers caused by disordering of the structure, such films are often amorphous or nanocrystalline [9]. On the other hand, introduction of reactive gas $O_2$ in process of sputtering suppresses formation of vacancies, promotes fuller oxidation of both In and Sn, but may result in formation of secondary phases (for example, SnO or $SnO_2$), which are not soluble in the lattice $In_2O_3$ [8]. Thus, the presence of $O_2$ in process of deposition of the film fundamentally changes the defect subsystem and distribution of the doping impurity.

Thermal annealing in the air atmosphere is a standard method to improve the crystallinity and activate the donors in ITO, however, the nature of the processes happening at the same time significantly depends on the initial phase and structural states, defined by the conditions of deposition. For the films produced in the inert atmosphere of Ar, annealing initiates recrystallization from the amorphous phase, growth of crystallites and complete integration of $Sn^{4+}$ into $In^{3+}$ positions [9]. At the same time the ITO films deposited with addition of oxygen contain stable oxide Sn phases and have a partially ordered structure [8], which in process of annealing may result in competing processes and phase-structural transitions.

Therefore, the purpose of this paper consists in establishment of the phase-structural transitions happening in thin ITO films in process of thermal annealing, and establishment of the effect from the presence of $O_2$ in process of deposition on the nature of such transitions.

## 2. Experiment method

### 2.1. Film deposition

ITO films with thickness of 150 nm are produced by direct-current (DC) magnetron sputtering from target $In_2O_3$:$SnO_2$ (90 : 10 wt.%) with diameter of 150 mm. Substrates were display glasses ($25 \times 25 \times 1.1$ mm). The distance to the target was 200 mm, the power was 400 W, the speed of deposition was $\sim 0.4$ nm/s. Sputtering was

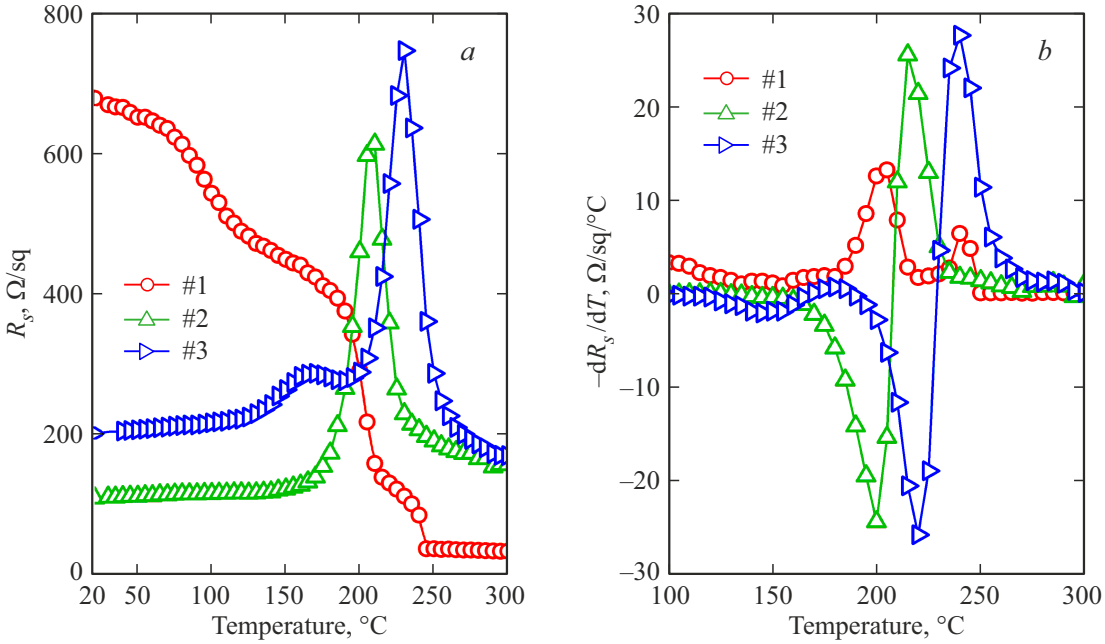



**Figure 1.** Dependence of surface resistance $R_s$ ($a$), derivative $dR_s/dT$ ($b$) on temperature in process of static annealing.

Studied samples

| Sample | Pressure, mTorr | Ar flow, $cm^3 \cdot min^{-1}$ | Flow $O_2$, $cm^3 \cdot min^{-1}$ | $R_s$, Ohm/square |
|---|---|---|---|---|
| #1 | 2.5 | 50 | – | $658 \pm 18$ |
| #2 | 1 | 50 | 1 | $107 \pm 2$ |
| #3 | 2.5 | 50 | 1 | $209 \pm 8$ |

carried out in Ar atmosphere with addition of $O_2$ for some samples. Deposition modes are provided in the table.

Control of thicknesses in real time is carried out by quartz sensors Inficon, and their calibration was carried out with ellipsometer Elli-SE and profilometer AMBIOS XP-200.

### 2.2. Measurement of surface resistance

Surface resistance $R_s$ was measured with a four pin probe JG ST2258C (error $\sim 0.5\%$ in the range of 50 $\mu$Ohm/square$-$1 $\mu$Ohm/square).

### 2.3. X-ray diffraction analysis

X-ray diffraction analysis was conducted on Bruker D8 Discover A25 DaVinci Design (Cu$K_{\alpha 1}$, $\lambda = 1.54178$Å).

### 2.4. Transmission electron microscopy

Images of transmission electron microscopy were obtained using a microscope Zeiss Libra 200 FE HR.

### 2.5. Thermal annealing

Thermal annealing was performed using a precision hot plate Tomanalit PL-01 with the temperature maintenance precision of 1 °C.

#### 2.5.1. Static annealing

The mode of static annealing presumed the measurement of $R_s$ in process of stepwise heating from room temperature $\sim 20$ °C to 300 °C with the pitch of 5 °C and holding time of 3 min per pitch.

#### 2.5.2. Dynamic annealing

The mode of dynamic annealing presumed measurement of $R_s$ with the interval of 1 min at fixed temperatures of 80, 195 and 245 °C.

## 3. Experimental findings

### 3.1. Electric properties of samples

Our primary objective was to study the change in surface resistance $R_s$ in samples #1, 2 and 3 in process of static annealing. Sample #1, applied in the inert atmosphere, demonstrated monotonic decrease in resistance to the temperature of 245 °C, and then no such changes were observed (Figure 1, $a$). High initial resistance specifies the amorphous structure after deposition, and considerable decrease of resistance with temperature growth ($dR_s/dT < 0$) (Figure 1, $b$) indicates the formation of the semiconductor crystalline microstructure. Despite the fact

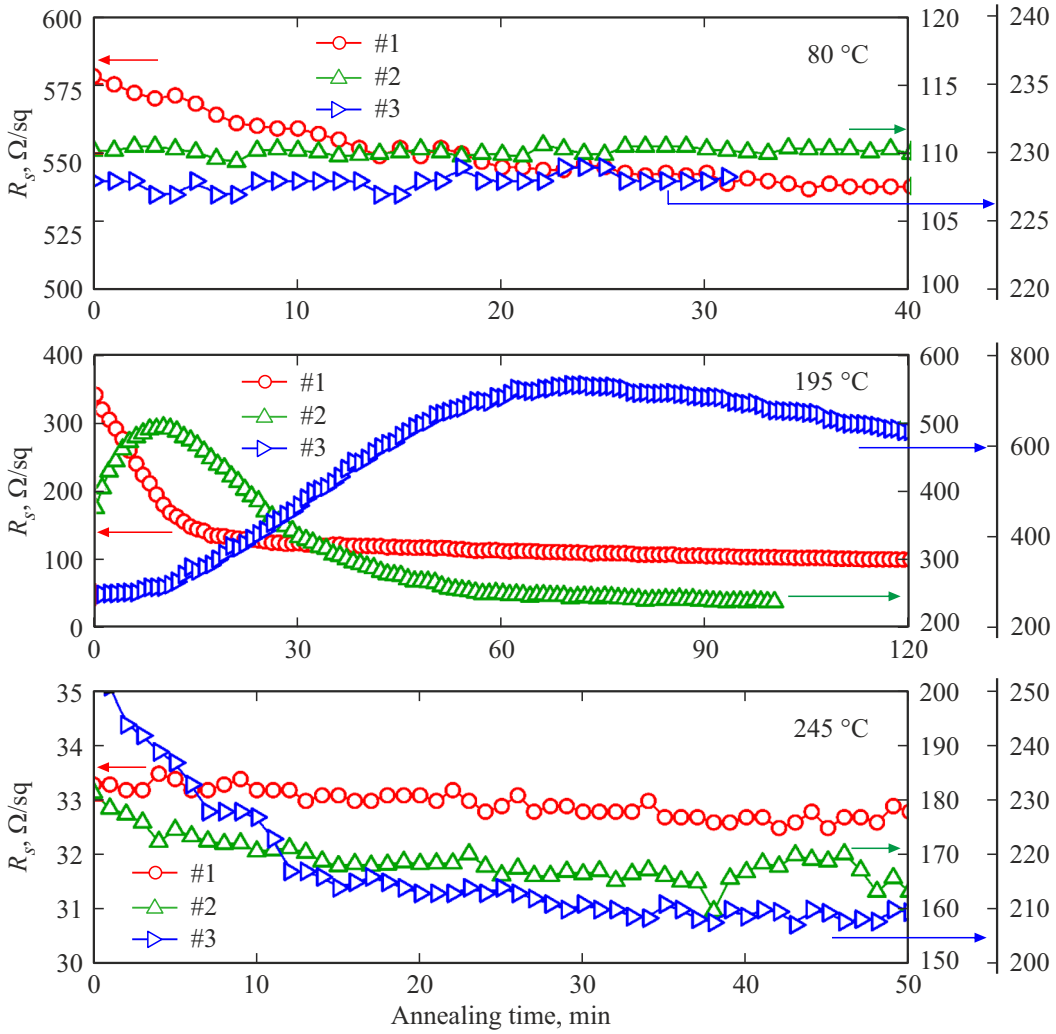



**Figure 2.** Dependence of surface resistance $R_s$ on time in process of dynamic annealing at temperatures of 80, 195 and 245 °C.

that samples #2 and 3 first had a relatively low $R_s$, as temperature increased, the resistance slightly increased, with dramatic rise at $\sim 160$ °C for #2 and $\sim 210$ °C for #3. The metal nature of conductivity ($dR_s/dT > 0$) persisted up to extrema, after which the rapid drop was observed in resistance up to the limit temperature $\sim 300$ °C, and the nature of conductivity after achievement of extrema became semiconductor ($dR_s/dT < 0$). This behavior is due to the initially formed microstructure of the samples, and the difference in temperatures of extrema for #2 and 3 is related to different partial pressures in process of deposition.

The change in the nature of dependence $dR_s/dT$ for samples #2 and 3 in the results of the static annealing is of special interest, namely, the transition from the metal conductivity to the typical semiconductor one, which may indicate phase structural readjustment in the ITO film. A change in the sign of the temperature resistance coefficient is explained by the fact that in the initial state the samples #2 and 3 are initially in the state with the metal type of conductivity, and after annealing above the extremum the concentration of carriers may decrease down to the non-degenerate level, and also potential barriers are formed on the boundaries of crystallites, which are specific for polycrystalline semiconductors, which causes a negative temperature coefficient of resistance.

For analysis of relaxation processes, we conducted the dynamic annealing at fixed temperatures of 80, 195 and 245 °C (Figure 2). At 80 °C the values $R_s$ of samples #2 and 3 remained unchanged, whereas in sample #1 the resistance dropped significantly in the first minutes, after which slow relaxation was observed. This indicates that already at 80 °C in sample #1 the recrystallization processes start, whereas in samples #2 and 3 at such temperature there are no significant changes. At 195 °C all three samples showed dependence $R_s$ on time: in #1 it drastically dropped, then continued decreasing further slowly; samples #2 and 3 behaved qualitatively similarly, but differed in time of achievement of extremum $R_s$. At 245 °C all samples demonstrated a slow drop $R_s$. Therefore, the result of dynamic annealing confirmed the transition

from the metal to semiconductor conductivity as a result of the structural phase readjustment in samples #2 and 3.

### 3.2. Microstructural properties of samples

To confirm the change in the microstructural properties, we performed X-ray diffraction analysis of samples #1 and 2 prior to static annealing at temperature 300 °C and afterwards (Figure 3). Prior to annealing, samples #1 and 2 contain no extrema corresponding to the specific ITO phases. Sample #1 is fully amorphous, which explains the presence of the high surface resistance $R_s$ prior to annealing (Figure 1, #1). Sample #2 shows formation of crystalline phase of SnO, which indicates partial oxidation of Sn in process of deposition and partial solubility in the ITO structure. This is exactly the phase that prevents the effective doping and maintains the metal type of conductivity at initial temperatures of annealing (Figure 1).

After annealing at 300 °C both samples acquire preferable orientations specific for the ITO pattern. In case of #1 peaks corresponding to SnO were not found, which indicates full solubility of Sn in the lattice $In_2O_3$, and in case of #2 these peaks remained unchanged, which indicates formation of resistant oxide clusters of tin in process of deposition in the oxygen-containing atmosphere. These clusters are not soluble at 300 °C and block the effective doping, therefore the end resistance of sample #2 remains higher than in #1. Moreover, the presence of the non-dissolved SnO phase correlates with the observed transition „metal–semiconductor", since the initial state ($dR_s/dT > 0$) is due to the defect structure with high concentration of carriers, and after annealing above the temperature extremum the concentration of carriers decreases, and potential barriers are formed on the boundaries of crystallites, which as a result causes semiconductor nature ($dR_s/dT < 0$).

To visualize the microstructure, the studies were conducted using the method of transmission electron microscopy. The image of sample #1 (Figure 4, *a*) shows a homogeneous finely dispersed structure with the blurred boundaries between the grains, which is specific for the amorphous or nanocrystalline state. The absence of the clear crystallographic contrasts and low contrast of the image indicate the low degree of atomic ordering. In case of sample #2 (Figure 4, *b*) the same amorphous microstructure is observed with inclusions of SnO-phases.

It should be noted that the presence of the secondary phase of SnO as such does not allow for unambiguous judgment on the concentration of the free charge carriers. The resulting electric properties of the films depend on both the quantity of tin within the solid solution $In_2O_3$ and the concentration of oxygen vacancies, distribution of defects, state of grain boundaries and the degree of material crystallinity. Therefore, the presence of SnO phase does not prevent the ability to observe the metal nature of the temperature dependence of resistance.

Therefore, the observed behavior of initial samples does not depend on a single factor, but rather on a combination

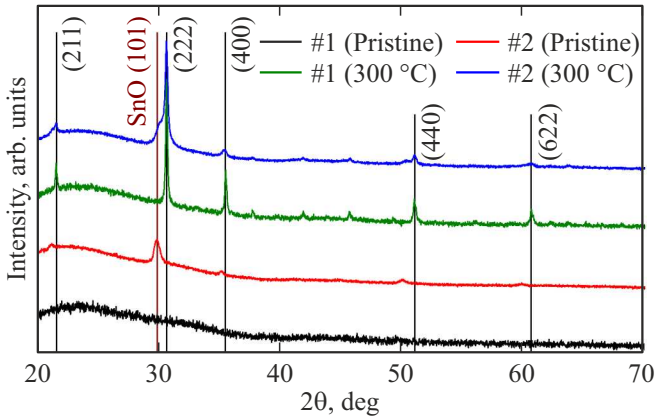



**Figure 3.** Results of X-ray diffraction analysis for samples #1 and 2 before and after annealing.

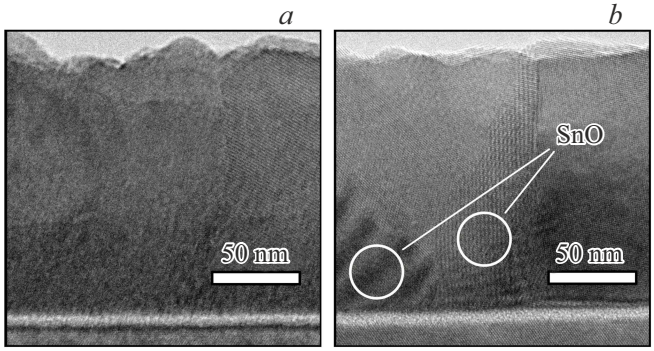



**Figure 4.** Images of transmission electron microscopy of samples #1 (*a*) and #2 (*b*) before annealing.

of the processes that include tin distribution between the solid phase $In_2O_3$ and secondary phase of SnO, presence of residual oxygen vacancies, features of the defect structure of the films, and also the state of grain boundaries. It is the joint impact of these factors that defines the effective concentration and mobility of charge carriers and, accordingly, the temperature dependence of resistance.

## 4. Conclusion

The study conducted the complex analysis of electric and microstructural properties of thin ITO films obtained by magnetron sputtering in the atmosphere of pure Ar and with addition of $O_2$, in process of static and dynamic annealing. It was established that the conditions of deposition define the initial phase state: inert atmosphere results in formation of amorphous semiconductor structure with low electroconductivity, and oxygen-containing one — to the formation of undissolved SnO phase and higher electroconductivity at the expense of the metal type of conductivity that transitions to the semiconductor one when annealed. Structural phase readjustment „metal–semiconductor" is due to the reduction in the concentration of carriers and formation of potential

barriers at boundaries of crystallites, whereas non-dissolved SnO clusters block the achievement of minimum resistance.

Therefore, the key factor that determines the electric behavior of ITO when annealed is the presence of stable oxide phases of tin, which arise when sputtered in the oxygen-containing environment. Deposition in pure argon makes it possible to fully avoid this effect and obtain the films with the maximum conductivity after annealing. The results establish a direct link between the conditions of synthesis, microstructure and type of conductivity, which is important for the targeted production of transparent electrodes with the specified properties.

### Funding

The study was conducted with the support of the grant of the Russian Science Foundation (project No. 26-19-00337).

### Conflict of interest

The authors state that they have no conflict of interest.

## References

[1] K. Ellmer. Nature Photonics, **6**, 809 (2012). https://doi.org/10.1038/nphoton.2012.282
[2] M. Morales–Masis, S. De Wolf, R. Woods–Robinson, J. Ager, C. Ballif. Adv. Electron. Mater., **3**, 1600529 (2017). DOI:10.1002/aelm.201600529
[3] N.S. Parashchuk, A.D. Kurilov, Yu.Ye. Bonyushkin, S.A. Stakharny, A.V. Nuriev, A.A. Morozov, D.N. Chausov. Infocommun. and Radio Technol., **10**, 16 (2024).
[4] A. Walsh, C. Richard A. Catlow. J. Mater. Chem., **20**, 10438 (2010). https://doi.org/10.1039/c0jm01816c
[5] A. Kosarian, M. Shakiba, E. Farshidi. IEEJ Trans. Electrical and Electronic Engin., **13**, 27 (2018). https://doi.org/10.1002/tee.22494
[6] S. Yang, J. Zhong, B. Sun, X. Zeng, W. Luo, X. Zhao, Y. Shu, J. Chen, J. He. J. Mater. Sci.: Mater. Electron., **30**, 13005 (2019). DOI: 10.1007/s10854-019-01662-w
[7] I. Hamberg, C.G. Granqvist. J. Appl. Phys., **60**, 123 (1986). DOI:10.1063/1.337534
[8] Yu.S. Zhidik, P.E. Troyan, V.V. Kozik, S.A. Kozyukhin, A.V. Zabolotskaya, S.A. Kuznetsova. Russian Phys. J., **63**, 1139 (2020). https://doi.org/10.1007/s11182-020-02167-4
[9] L.P. Amosova. Semiconductors, **49**, 414 (2015).

*Translated by D.Safin*